J|A|C|S
ARTICLES
Published on Web 02/16/2008

Site-Specific Relaxation Kinetics of a Tryptophan Zipper Hairpin Peptide Using Temperature-Jump IR Spectroscopy and Isotopic Labeling

Karin Hauser,*[,#] Carsten Krejtschi,[#] Rong Huang,[†] Ling Wu,[†] and Timothy A. Keiderling[†]

Institut für Biophysik, Johann Wolfgang Goethe-Universität Frankfurt, Max-von-Laue-Strasse 1, 60438 Frankfurt, Germany, and Department of Chemistry, University of Illinois at Chicago, 845 W. Taylor Street, Chicago, Illinois 60607-7061

Received June 9, 2007; E-mail: hauser@biophysik.uni-frankfurt.de

Abstract: Two antiparallel β-strands connected by a turn make β-hairpins an ideal model system to analyze the interactions and dynamics of β-sheets. Site-specific conformational dynamics were studied by temperature-jump IR spectroscopy and isotopic labeling in a model based on the tryptophan zipper peptide, Trpzip2, developed by Cochran et al. (*Proc. Natl. Acad. Sci. U.S.A.* **2001**, *98*, 5578). The modified Trpzip2C peptides have nearly identical equilibrium spectral behavior as Trpzip2 showing that they also form well-characterized β-hairpin conformations in aqueous solution. Selective introduction of $^{13}C{=}O$ groups on opposite strands lead to distinguishable cross-strand coupling of the labeled residues as monitored in the amide I′ band. These frequency patterns reflect theoretical predictions, and the coupled $^{13}C{=}O$ band loses intensity with increase in temperature and unfolding of the hairpin. Thermal relaxation kinetics were analyzed for unlabeled and cross-strand isotopically labeled variants. T-jumps of ~10 °C induce relaxation times of a few microseconds that decrease with increase of the peptide temperature. Differences in kinetic behavior for the loss of β-strand and gain of disordered structure can be used to distinguish localized structure dynamics by comparison of nonlabeled and labeled amide I′ components. Analysis of the data supports multistate dynamic and equilibrium behavior, but because of this process it is not possible to clearly define a folding and unfolding rate. Nonetheless, site-specific relaxation kinetics could be seen to be consistent with a hydrophobic collapse hypothesis for hairpin folding.

Introduction

Understanding protein folding is a challenge of fundamental importance in biophysics and furthermore is of growing biomedical relevance since misfolded proteins are found to be diagnostic of a growing number of disease states.[1] Second only to α-helices, β-sheets are one of the main extended structural elements in proteins yet pose difficulties for study of folding mechanisms because of their variable structures and propensity for aggregation. β-hairpins, composed of two antiparallel strands connected by a turn, provide ideal model systems for study of a monomeric, well-defined structure containing a sheet segment, and probably are important structural elements in the initiation of sheet formation. It is still unclear whether hairpin folding itself is initiated by sequence propensities to form a turn and bring the strands together or by cross-strand interaction of residues to stabilize a compact state and allow the turn to form.[2−4] The latter is normally attributed to a hydrophobic collapse and is aided by sequence design, placing nonpolar residues on alternate positions in the cross-strand segments to interact and thereby exclude water from one side of the extended structure.

IR spectroscopy can monitor local secondary structure changes on different time scales by probing the amide I′ region with equilibrium and dynamics techniques. We and others have shown that site-specific isotope labeling can enable IR detection of localized conformational changes.[5−18] Specific sites in a sheet

[#] Johann Wolfgang Goethe-Universität Frankfurt.
[†] University of Illinois at Chicago.

(1) Zurdo, J. *Protein Pept. Lett.* **2005**, *12*, 171−187.
(2) Deechongkit, S.; Nguyen, H.; Jager, M.; Powers, E. T.; Gruebele, M.; Kelly, J. W. *Curr. Opin. Struct. Biol.* **2006**, *16*, 94−101.
(3) Searle, M. S.; Ciani, B. *Curr. Opin. Struct. Biol.* **2004**, *14*, 458−464.
(4) Du, D.; Tucker, M. J.; Gai, F. *Biochemistry* **2006**, *45*, 2668−2678.
(5) Setnička, V.; Huang, R.; Thomas, C. L.; Etienne, M. A.; Kubelka, J.; Hammer, R. P.; Keiderling, T. A. *J. Am. Chem. Soc.* **2005**, *127*, 4992−4993.
(6) Silva, R. A. G. D.; Kubelka, J.; Bouř, P.; Decatur, S. M.; Keiderling, T. A. *Proc. Natl. Acad. Sci. U.S.A.* **2000**, *97*, 8318−8323.
(7) Bouř, P.; Keiderling, T. A. *J. Phys. Chem. B* **2005**, *109*, 5348−5357.
(8) Huang, C.-Y.; Getahun, Z.; Wang, T.; Degrado, W. F.; Gai, F. *J. Am. Chem. Soc.* **2001**, *123*, 12111−12112.
(9) Fesinmeyer, R. M.; Peterson, E. S.; Dyer, R. B.; Andersen, N. H. *Protein Sci.* **2005**, *14*, 2324−2332.
(10) Hauser, K.; Engelhard, M.; Friedman, N.; Sheves, M.; Siebert, F. *J. Phys. Chem.* **2002**, *106*, 3553−3559.
(11) Fesinmeyer, R. M.; Hudson, F. M.; Olsen, K. A.; White, G. W. N.; Euser, A.; Anderson, N. H. *J. Biomol. NMR* **2005**, *33*, 213−231.
(12) Brauner, J. W.; Dugan, C.; Mendelsohn, R. *J. Am. Chem. Soc.* **2000**, *122*, 677−683.
(13) Kubelka, J.; Keiderling, T. A. *J. Am. Chem. Soc.* **2001**, *123*, 12048−12058.
(14) Silva, R. A. G. D.; Barber-Armstrong, W.; Decatur, S. M. *J. Am. Chem. Soc.* **2003**, *125*, 13674−13675.
(15) Huang, R.; Kubelka, J.; Barber-Armstrong, W.; Silva, R. A. G. D.; Decatur, S. M.; Keiderling, T. A. *J. Am. Chem. Soc.* **2004**, *126*, 2346−2354.
(16) Paul, C.; Wang, J.; Wimley, W. C.; Hochstrasser, R. M.; Axelsen, P. H. *J. Am. Chem. Soc.* **2004**, *126*, 5843−5850.

10.1021/ja074215l CCC: $40.75

structure have been shown to have unique cross-strand coupling interactions[7,19,20] that yield distinctive isotope-shifted bands for the amide I′ mode. We have used such couplings to probe folding in a hairpin model stabilized by a uniquely designed turn sequence.[5,21]

Cochran et al. developed the tryptophan zipper (Trpzip) sequences that are stabilized by Trp−Trp cross-strand interaction and form well-characterized β-hairpin conformations in aqueous solution.[22] Their study used CD to determine thermal stability of the Trp−Trp interactions and NMR to develop a solution structure. While CD and fluorescence studies can only address tertiary structure changes in Trpzip structures, since amide contributions are fully overlapped by Trp $\pi-\pi^*$ transitions in the far-UV−CD, IR offers a means of obtaining unique insight into the secondary structure. Spectroscopic studies on different Trpzip variants have shown both equilibrium and dynamic changes in structure with variation in temperature and have been interpreted in different ways.[23−29]

In this paper, we present the first site-specific temperature-jump (T-jump) IR kinetic data for cross-strand isotopically labeled hairpin peptides. These tryptophan zipper hairpins are designed to be a derivative (mutant) of Trpzip2, originally proposed by Cochran and co-workers,[22] and are additionally labeled with ^{13}C on selected amide C═O positions on opposite strands. The isotopic patterns were chosen based on results we have recently reported using both theoretical models and equilibrium IR studies of various isotopically labeled sequences for a different 12-residue hairpin, in that case stabilized by turn residues.[5,19−21] Here, we provide new site-specific kinetic information on the folding and unfolding processes for this Trpzip variant based on background equilibrium studies.

Experimental Section

Peptide Synthesis. Peptides were synthesized in the UIC Research Resources Protein Lab using a standard automated synthesizer with normal FMOC-based solid-state synthesis methods. To achieve isotopic labeling, blocked residues that were ^{13}C-labeled on C1 (amide C═O) were purchased from Cambridge Isotope Laboratories and used directly with the synthesizer. After trifluoroacetic acid (TFA) cleavage from the resin, the crude preparations were purified with HPLC and their identity confirmed with MALDI MS. The peptide sequence studied is termed Trpzip2C, a variant of Trpzip2 with Ser1, Thr3, and Thr10 substituted by Ala (shown schematically in Scheme 1), a mutation that has little impact on the structure or stability of the target hairpin, which we have tested by comparison of their CD and IR bandshapes as well as NMR behavior (see Results).[22,23,27] The solubility is slightly reduced, but we were able to define conditions, acidic pH, and modest concentration, allowing the samples to dissolve and reversibly fold while providing solutions of sufficient spectral absorbance for our studies. The Ala substitutions provide ideal positions for labeling at reasonable cost in terms of reagents for the synthesis. Unlabeled as well as doubly labeled peptides were prepared with ^{13}C substituted on the C1 position (the amide C═O) of the designated residue in sequences denoted **A1A10**, **A3A10**, and **A3K8** (defined in Table 1) and interacting as indicated in Scheme 1.[30]

Scheme 1. Sequences Showing Trpzip2C Peptides (variants of Trpzip2 with the Three Ala Substitutions (S1A, T3A, and T10A)) Which We Have Studied as Unlabeled and Doubly Labeled Variants Designated As **A1A10** (green), **A3A10** (blue), and **A3K8** (red), Labeled with ^{13}C on the Marked Amide C═O

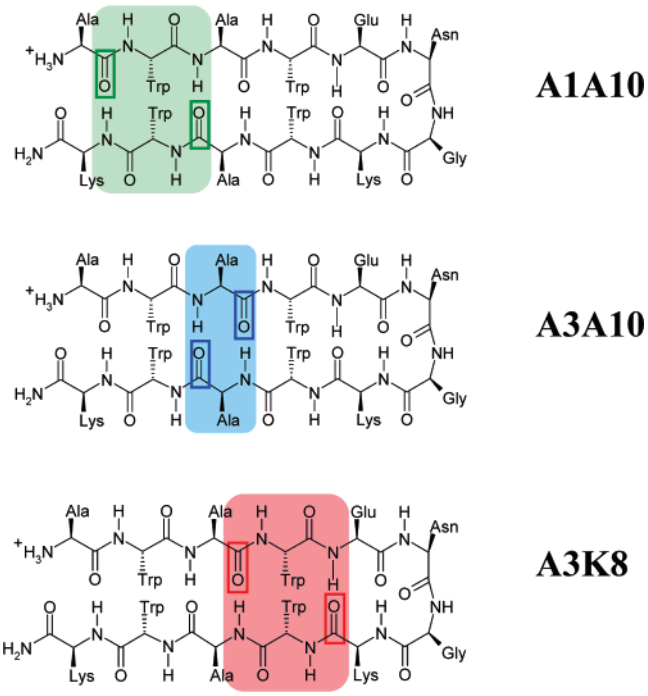

Table 1. Comparative Sequences of Peptides Studied[a]

peptide	sequence
Trpzip2	SWTWENGKWTWK-NH_2
Trpzip2C	AWAWENGKWAWK-NH_2
A1A10	A*WAWENGKWA*WK-NH_2
A3A10	AWA*WENGKWA*WK-NH_2
A3K8	AWA*WENGK*WAWK-NH_2

[a] Residues marked with * are labeled with ^{13}C on the amide C═O.

CD and FTIR Studies in Thermal Equilibrium. Measurements in thermal equilibrium were carried out with CD and FTIR. CD measurements at UIC used a JASCO 810 spectropolarimeter with a standard 1 mm path quartz cell coupled to a Neslab water bath to provide temperature control as has been described.[21,30] CD samples were dissolved in 20 mM phosphate buffer at ∼0.2 mg/mL (∼110 μM) with no further purification, and HCl was added to adjust pH. The amplitude variation with temperature was fit to a two-state model assuming a linear folded and flat unfolded baseline with $\Delta C_p = 0$.[21,30] Attempts to include ΔC_p in the fit resulted in statistically unreliable values (zero within the error).

FTIR equilibrium studies were carried out both in Chicago and Frankfurt on Digilab FTS-60A and Bruker Equinox 55 FTIR instruments, respectively, to prove consistency and demonstrate that the

(17) Huang, C.-Y.; Getahun, Z.; Zhu, Y.; Klemke, J. W.; Degrado, W. F.; Gai, F. *Proc. Natl. Acad. Sci. U.S.A.* **2002**, *99*, 2788−2793.
(18) Brauner, J. W.; Flach, C. R.; Mendelsohn, R. *J. Am. Chem. Soc.* **2005**, *127*, 100−109.
(19) Kim, J.; Huang, R.; Kubelka, J.; Bour, P.; Keiderling, T. A. *J. Phys. Chem. B* **2006**, *110*, 23590−23602.
(20) Bour, P.; Keiderling, K. *J. Phys. Chem. B* **2005**, *109*, 23687−23697.
(21) Huang, R.; Setnička, V.; Etienne, M. A.; Kim, J.; Kubelka, J.; Hammer, R. P.; Keiderling, T. A. *J. Am. Chem. Soc.* **2007**, *129*, 13592−13603.
(22) Cochran, A. G.; Skelton, N. J.; Starovasnik, M. A. *Proc. Natl. Acad. Sci. U.S.A.* **2001**, *98*, 5578−5583. Correction: *Proc. Natl. Acad. Sci. U.S.A.* **2002**, *99*, 9081−9082.
(23) Wang, T.; Xu, Y.; Du, D.; Gai, F. *Biopolymers* **2004**, *75*, 163−172.
(24) Smith, A. W.; Chung, H. S.; Ganim, Z.; Tokmakoff, A. *J. Phys. Chem. B* **2005**, *109*, 17025−17027.
(25) Smith, A. W.; Tokmakoff, A. *J. Chem. Phys.* **2007**, *126*, 045109.1 −11.
(26) Yang, W. Y.; Gruebele, M. *J. Am. Chem. Soc.* **2004**, *126*, 7758−7759.
(27) Yang, W. Y.; Pitera, J. W.; Swope, W. S.; Gruebele, M. *J. Mol. Biol.* **2004**, *336*, 241−251.
(28) Du, D.; Zhu, Y.; Huang, C.-Y.; Gai, F. *Proc. Natl. Acad. Sci. U.S.A.* **2004**, *101*, 15915−15920.
(29) Snow, C. D.; Qiu, L.; Du, D.; Gai, F.; Hagen, S. J.; Pande, V. S. *Proc. Natl. Acad. Sci. U.S.A.* **2004**, *101*, 4077−4082.
(30) Huang, R. Ph.D. Thesis, University of Illinois at Chicago, Chicago, IL, 2007.

samples were not subject to decay or to unfolding in storage or transition between labs. The samples were held in homemade cells having CaF_2 windows separated with a 100 μm spacer and thermostated by a regulated water flow from a temperature controlled bath through a cell holder. The temperature program and data collection were automated and programmed to allow for equilibration after each temperature step. Equilibrium IR measurements have been carried out at different pH values and also served to determine reversible un/refolding conditions and to select the probe wavelengths for the T-jump measurements. Low pH samples had higher solubility and gave more reversible thermal IR data; thus, those conditions were chosen for T-jump experiments. The samples were dissolved in 0.1 M DCl and lyophilized three times to remove TFA counterions remaining from the peptide synthesis. The final solutions were then prepared by redissolving in D_2O and adjusting pH with DCl.

Temperature-Jump Measurements. T-jump experiments were realized with a home-built spectrometer developed in Frankfurt and is described in more detail separately.[31] Rapid heating of the solvent is induced by a Raman-shifted Nd:YAG laser pulse (10 ns) that excites an overtone vibration of D_2O at 1909 nm by use of a Nd:YAG Laser (Spectron SL454G, England), 650 mJ at 1064 nm and a Raman shifter (Radiant Dyes, Germany) filled with 30 bar of H_2. The 1909 nm excitation beam was split into two components, one delayed by approximately 10 ns, and used to excite the sample from the front and back side of the sample cell with two counter-propagating heating pulses, which leads to a more homogeneous heating profile and helps control cavitation.[32] The beams were focused beyond the sample to avoid high power densities on the surface.[33] Their absorption by the solvent initiates the T-jump and increases the sample temperature in the cell by approximately 10 °C. Cryogenically cooled lead salt laser diodes (Laser Components, Germany) operating in a continuous wave (cw) mode provided a single-wavelength IR source tunable in a spectral region from 1580 cm^{-1} to 1700 cm^{-1}. Multiple modes are emitted, necessitating isolation of the probe frequency by use of a monochromator (Mütek TLS 310, Germany). The transient transmission was measured with a photovoltaic 20 MHz MCT detector (Kolmar Technologies KMPV11-1-J2, MA) and digitized by a transient recorder board (Imtec T3012, Germany). The same cells were used as described above for the equilibrium experiments, connected to a temperature controlled water bath (Lauda Ecoline E300, Germany), and the sample was equilibrated to a defined temperature. The samples were measured at acidic pH (~1.1) and a concentration of 20 mg/mL.

After application of the fast T-jump ($\Delta T \sim 10$ °C), the spectral response was monitored as a function of time at single wavelengths in the amide I′ region. At least 2000 single absorption transients were averaged to yield decay curves for several temperatures at each probed wavelength. The observed transients reflect both peptide and solvent contributions. We used a biexponential model ($\Delta A(t) = A_0 + A_1 \exp(-t/\tau_1) + A_2 \exp(-t/\tau_2)$) to decompose the kinetics of the peptide relaxation and the solvent cooling, each represented with a monoexponential decay function. Because of its relatively slow cooling rate (ms), change in the water absorbance has minimal interference over the time scale of Trpzip2C unfolding (μs). Since the cooling of the solvent becomes strongly nonexponential for longer time scales,[34] we restricted the fit to the time interval between 500 ns to 180 μs. Data within the first 500 ns after the T-jump was adversely impacted by perturbations on the instrument electronics and thus was omitted from data analysis. This approach encompasses the time scale of Trpzip2C relaxation and provides a means of solvent correction for each data set by eliminating variations in temperature and path length that could affect sequential measurements. T-jump measurements were performed starting from different temperatures of the sample as controlled by the water bath.

Results

Equilibrium Properties. The Trpzip2C sequence has nearly the same stability as the Trpzip2 parent, as demonstrated by its unfolding transition (monitored by CD) having a T_m of 344 ± 2 K at pH 6.9, using the methods described above, which is essentially identical to that reported for Trpzip2 (345 K). At lower pH (which was used for the T-jump experiments in this study to obtain improved reversibility), the T_m value dropped to 335 ± 2 K. The spectral shapes of the Trpzip2C CD and IR spectra are virtually identical with that of the Trpzip2 parent compound (see Figures 1 and 2), implying that the variant is folded in the same way as the parent at low temperature. All labeled variants had identical UV−CD spectra, and their temperature dependencies were fully the same as seen in Figure 1, showing that they had consistent folds and overall stabilities.

The IR absorption maximum shifted from 1633 cm^{-1} to 1649 cm^{-1} as temperature increased from 5 to 85 °C for the unlabeled peptide (see Figure 2; precise wavenumber values were affected by baseline correction) corresponding to a secondary structural change correlated with the CD-detected tertiary change (Figure 1). This IR-detected thermal behavior for Trpzip2C secondary structure also follows that of Trpzip2 in the IR (based on our unpublished results for Trpzip2). IR spectra just show the amide I′ band without TFA, a common contaminant of the synthesis and cleavage from the resin that we have removed, and that appears to have been present in some earlier Trpzip2 IR studies, resulting in an interfering band at ~1672 cm^{-1}.[27] The thermal variation for the ^{12}C bands of the labeled peptides were similar (Figure 3), except that the frequencies were shifted due to the impact of the ^{13}C substitution on the ^{12}C coupling. These spectra can be analyzed directly in terms of frequency shift or intensity variation to yield thermal equilibrium curves and transition characteristics. The resulting T_m values for the intensity change only roughly match the CD result; however, those obtained from absorbance intensity changes at 1632 cm^{-1} and 1652 cm^{-1} do not agree (see Figure 2) and are quite dependent on the assumptions used in approximating the baseline, indicating that their uncertainties are more substantial than the fitting precision (~±2 K) and demonstrating that these transitions are not simple two-state processes.

NMR spectra of Trpzip2C showed a pattern of C_α chemical shifts characteristic of β-strand formation for residues 2−5 and 8−11, following our assignment of the spectra (L. Wu, D. McElheny, unpublished results), and turn formation in residues 6−7, as the hairpin was originally designed by Cochran, et al.[22] Where comparable, the pattern of chemical shifts (C_α-H) follows that described previously for Trpzip2, especially when analyzed in terms of chemical shift indexing to characterize changes from random coil values.[22] Because of the triple Ala substitution made for Trpzip2C and the four Trps, there is considerable degeneracy in the spectrum. Although NOEs between the Trp indole rings can be identified, sufficient unique assignments for a reliable structure determination have not yet been determined. In confirming hairpin formation, this NMR result is redundant with the CD and IR observations, but it does provide ancillary evidence for the conformation with this altered sequence.

As we have seen for other hairpin systems,[5,19−21] if we double label the peptide on the nearest cross-strand interacting pair of

(31) Krejtschi, C.; Huang, R.; Keiderling, T. A.; Hauser, K. *Vib. Spectrosc.* **2008**, in press.
(32) Wray, W. O.; Aida, T.; Dyer, R. B. *Appl. Phys. B* **2002**, *74*, 57−66.
(33) Ballew, R. M.; Sabelko, J.; Reiner, C.; Gruebele, M. *Rev. Sci. Instrum.* **1996**, *67*, 3694−3699.
(34) Ramajo, A. P.; Petty, S. A.; Volk, M. *Chem. Phys.* **2006**, *323*, 11−23.

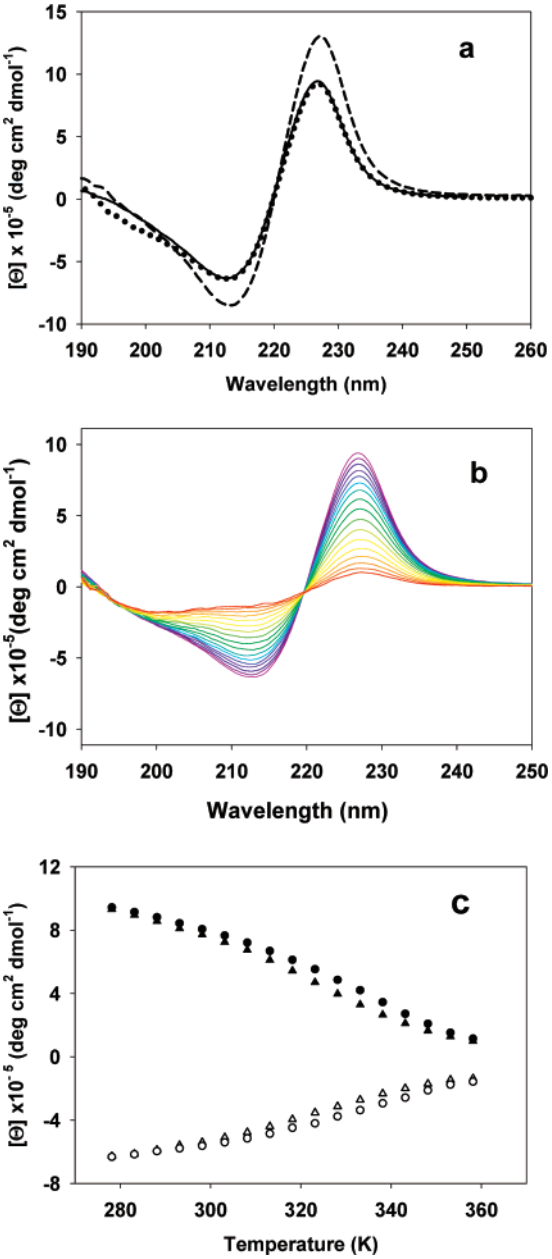

Figure 1. CD spectra and thermal stability of Trpzip2C at neutral vs acidic pH. (a) overlap of spectra for Trpzip2C at low (2.4; dotted line) and neutral pH (6.9; solid line) with that of Trpzip2 at neutral pH (dashed line). (b) Variation of CD with temperature for Trpzip2C in water at pH 2.4, showing the magnitude decreases with change from 5 (blue) to 85 °C (red). (c) Analyses of the thermal change by measuring the CD intensity at 227 (decreasing, solid symbols) and 213 nm (increasing, open symbols). Circles indicate pH 6.9, triangles, pH 2.4, and the deviation in the two curves reflects their difference in T_m = 344 and 335 K, respectively. Actual temperature variation data shown are for A3K8, which will not affect the Trp−Trp tertiary structure or its stability. Plots are in molar ellipticity on a per molecule basis.

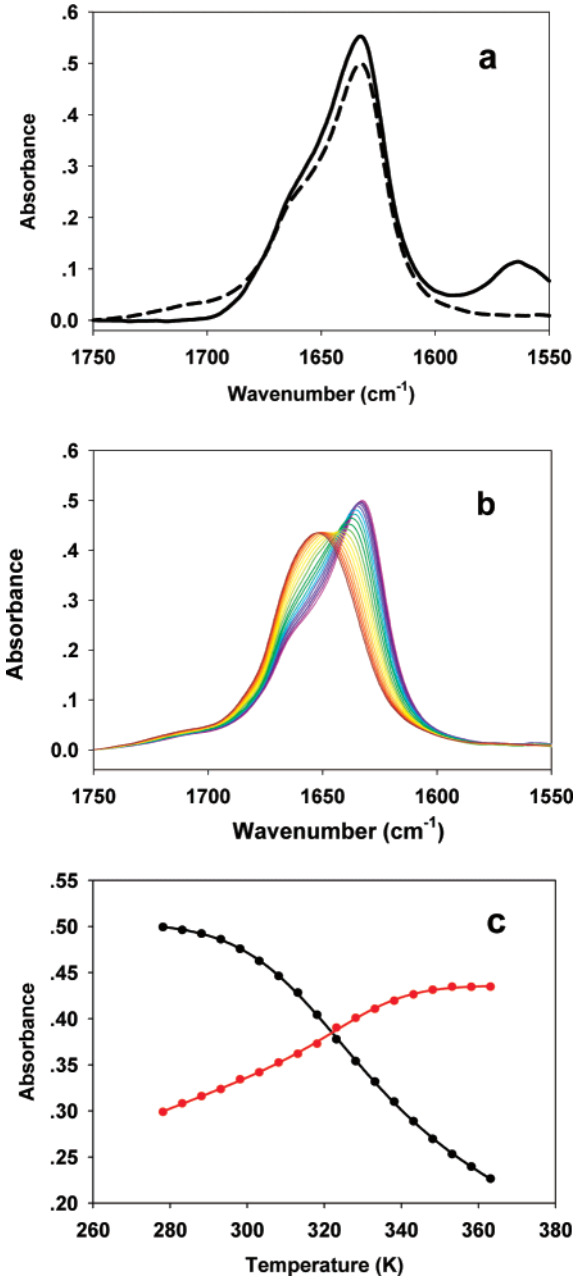

Figure 2. (a) Overlap of Trpzip2C amide′ IR at neutral (solid) and acidic (dashed line) pH (similar concentrations) showing near identical bandshapes which highlight their β-strand structure (the band at ∼1710 cm^{-1} at low pH results from the ν(C═O) stretching vibration of the protonated carboxyl groups (COOH), while that at ∼1570 cm^{-1} at neutral pH results from the antisysmmetric stretching vibration of the deprotonated carboxylate groups (COO$^-$)). (b) Temperature-dependent IR spectra of Trpzip2C at acidic pH, with an increase from 5 (blue) to 85 °C (red) in steps of 5 °C. (c) Fit of IR intensity change at 1632 cm^{-1}, correlated to β-sheet contribution (black circles), and 1652 cm^{-1}, correlated to disordered contribution (red circles), to a two-state model yielding apparent transition temperatures of 321 and 333 K, respectively, which are quite dependent on baseline assumptions used in the model.

amide C═O groups, their vibrational frequencies will shift and their unique coupling will result in a pattern characteristic of their relative structure, as seen for the low-temperature IR spectra of the labeled peptides shown in Figure 3. In the **A3A10** peptide the ^{13}C═O groups form a 10-member H-bonded ring and the frequency of the isotope-shifted mode is ∼1608 cm^{-1}, while for the **A3K8** peptide the labeled groups form a 14-member ring and the frequency is ∼1615 cm^{-1}. The difference arises because the two types of C═O pairs have oppositely signed coupling constants, and because of the out-of-phase mode having most of the intensity (since it creates the larger transition dipole), the observed ^{13}C═O transitions appear at different frequencies, as we have shown in various theoretical models.[5,19−21] This phase difference means that the **A3A10** band shifts down from the position for a single label while that for **A3K8** shifts up, giving them an observed wavenumber difference of 7 cm^{-1}.

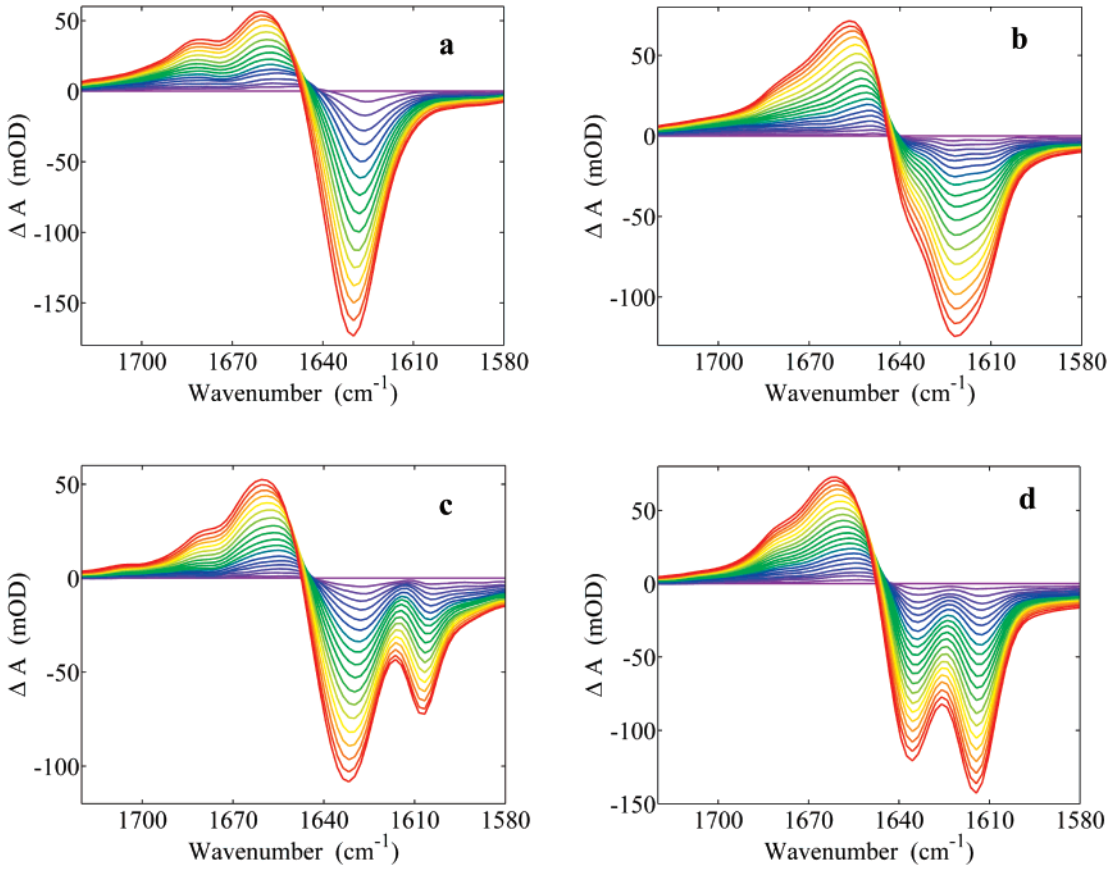

Figure 3. Temperature-dependent IR difference spectra of unlabeled and double-labeled Tripzip2C peptides reflecting thermal unfolding (pH ∼ 1.1; referenced to the 5 °C spectrum; direction of increasing temperature goes from 5 (blue) to 85 °C (red)): (a) unlabeled; (b) **A1A10**; (c) **A3A10**; (d) **A3K8**. This differential representation is particularly useful for selecting wavenumbers to tune the probe laser for the T-jump experiment.

Our quantum mechanical theoretical approaches to spectral simulation have shown that this pattern occurs in a variety of hairpin structures and is qualitatively predictable with even simple, transition dipole coupling based models.[7,19,20] The larger rings always yield higher intensity $^{13}C{=}O$ sidebands on the amide I but smaller shifts from the $^{12}C{=}O$ modes than do the smaller rings, presumably due to differences in residual coupling to the $^{12}C{=}O$ modes. Our low-temperature equilibrium data for **A3A10** and **A3K8** show this phenomenon and fully match the computed $^{13}C{=}O$ amide I frequency patterns and band shapes found in other hairpin systems.[5,7,19,21] Such consistency confirms the in-register formation of the hairpin cross-strand H-bonds and provides further evidence for the well-formed hairpin nature of this Trpzip2C model system.

On the other hand, the **A1A10** variant does not fit this coupling model, and its spectra show the effects of fraying of the hairpin in the region of the terminal residues. Two bands characteristic of the $^{13}C{=}O$ labeling are seen at ∼1626 and 1614 cm^{-1}. This behavior has been shown to be characteristic of uncoupled residues (Huang and Keiderling, to be published).[30] Theoretical simulations of spectra for structural models of hairpins derived from MD calculations show a loss of coupling as the termini fray (Kim and Keiderling, unpublished).[19,21] The selection of labeled peptides thus permits us to explore separately the dynamic behavior in the well-formed strand region and in the less structured terminal region.

T-Jump Dynamics. This paper presents the first T-jump temperature dependence for cross-strand isotopically labeled hairpins. Here, Trpzip2C dynamics are compared to those of its labeled **A1A10**, **A3A10**, and **A3K8** variants. Relaxation kinetics upon thermal unfolding for unlabeled Trpzip2C were probed at various amide I′ frequency positions representing the decay of the folded peptide and the rise of the disordered structure. Temperature jumps of ∼10 °C have been applied at different temperatures, and relaxation times have been determined. Wavelength selection was based on optimal overlap of the maximum absorbance change as seen in the difference spectra (Figure 3) and intense modes of the lead salt diodes. Figure 4 shows the results of the variation in dynamic behavior for the unlabeled Trpzip2C probed at characteristic $^{12}C{=}O$ amide I′ modes representing the β-hairpin decay (1625 cm^{-1}) and rise in disordered structure (1661 cm^{-1}), respectively. Other wavelength positions within the broad amide I′ band have also been probed and showed analogous behavior as those extracted as representative examples in Figures 4 and 5. The relaxation time τ_{obs} occurs in a few microseconds and is of a similar magnitude as observed for Trpzip2 by Snow et al.[29] The relaxation time was determined as described in the Experimental Section and corresponds to the inverse of the rate constant, $k_{obs}{}^{-1}$. If this corresponded to a two-state kinetic model, k_{obs} would be the sum of the folding and unfolding rates, $k_{obs} = k_f + k_u$, even though the T-jump primarily induces unfolding of the peptide. For a two-state process, the folding rate could be derived from the observed relaxation as $k_f = k_{obs}/(1 + K_{eq}{}^{-1})$, if the equilibrium constant, $K_{eq} = k_f/k_u$, were known, or obtained from thermal equilibrium measurements, and the unfolding rate

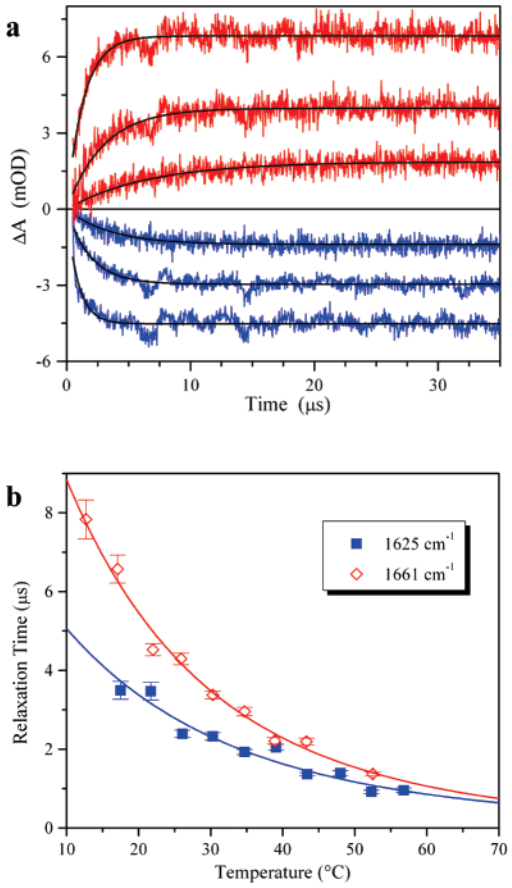

Figure 4. Dependence of relaxation kinetics on final peptide temperature for unlabeled Trpzip2C upon 10 °C T-jump. Blue traces represent the decay of the β-hairpin, probed at 1625 cm^{-1}, whereas red represent the rise of the disordered structure, probed at 1661 cm^{-1}. Relaxation times decrease with increasing peptide temperature. (a) Relaxation transients after water subtraction, for three selected temperatures (from top to bottom): (red) the rise of disordered structure at 52 °C ($\tau_{obs} = 1.4 \pm 0.1$ μs), 35 °C ($\tau_{obs} = 3.0 \pm 0.1$ μs), 17 °C ($\tau_{obs} = 6.6 \pm 0.4$ μs); (blue) the decay of β-hairpin at 17 °C ($\tau_{obs} = 3.5 \pm 0.2$ μs), 35 °C ($\tau_{obs} = 1.9 \pm 0.1$ μs), 52 °C ($\tau_{obs} = 0.9 \pm 0.1$ μs). More data is listed in Table 2. (b) Variation of relaxation time following the T-jump as a function of final peptide temperature for detection at 1625 cm^{-1} (blue squares) and 1661 cm^{-1} (red diamonds). Data points were fit to the Arrhenius equation as indicated in Table 3.

can be derived from k_f and either k_{obs} or K_{eq}. Since K_{eq} is very sensitive to the parameters chosen for the fit, we have seen considerable variation in the values determined and consequently have chosen to compare experiments and isotopic variants on the basis of the observed relaxation times, τ_{obs} ($= k_{obs}^{-1}$).

As shown in Figure 4, the relaxation time depends on the peptide temperature and increases with decreasing temperature. At temperatures >40 °C, there is little discrimination between relaxation times for different bands. However, at low temperatures, the relaxation times determined for the band components show that the band related to the β-strand (1625 cm^{-1}) decays faster than the band related to the disordered structure (1661 cm^{-1}) appears. Such low temperature behavior is inconsistent with a two-state unfolding mechanism (see Discussion).

The labeled β-hairpins have resolved $^{13}C{=}O$ bands that provide a site-specific probe of the dynamics of the Trpzip2C hairpin. Local differences are revealed by use of relative T-jump relaxation rates probed at selected frequencies: **A1A10** (1616 cm^{-1}), **A3A10** (1610 cm^{-1}), and **A3K8** (1618 cm^{-1}). Since the

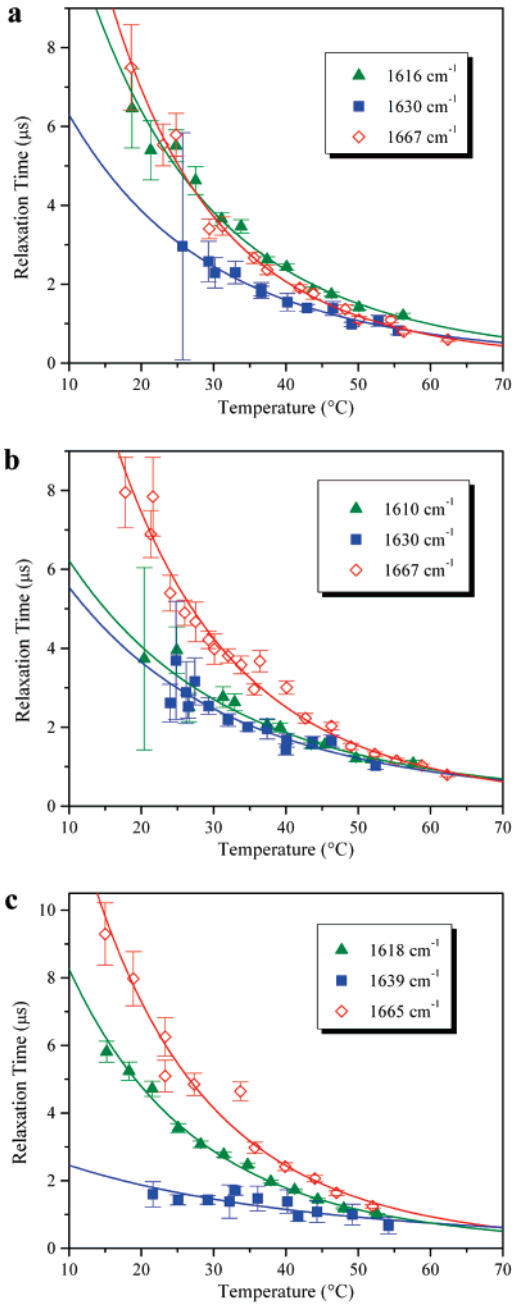

Figure 5. Dependence of the relxation time on final peptide temperature for isotopically labeled Trpzip2C variants upon ~10 °C T-jump. Red traces represent the rise of the disordered structure (1665−1667 cm^{-1}), blue the decay of the β-hairpin $^{12}C{=}O$ amide I′ mode (1630−1639 cm^{-1}), and green the decay of the $^{13}C{=}O$ amide I′ mode (1610−1618 cm^{-1}), for the labeled Trpzip2C variants: (a) **A1A10**; (b) **A3A10**; (c) **A3K8**. Data points were fit to the Arrhenius equation as indicated in Table 3. Selected relaxation times are listed in Table 2.

labels are introduced at different positions of the hairpin, stability variations at different positions can be observed from different kinetic behavior depending on the label location. Figure 5 shows representative variations of relaxation times with temperature obtained for different probe wavelengths corresponding to the $^{13}C{=}O$ amide I′ modes (green traces), $^{12}C{=}O$ amide I′ β-strand component (blue traces), and the disordered structure component (red traces) for each labeled variant. At low temperature, the transient absorbance changes are small, making the signals less reliable, which is the reason for the missing data points at low

Table 2. Comparison of Selected Relaxation Times (μs) of **A1A10**, **A3A10**, and **A3K8** at Similar Temperatures ($\pm$2 °C)

	A1A10			A3A10			A3K8		
	^{12}C-strand	^{13}C	disordered	^{12}C-strand	^{13}C	disordered	^{12}C-strand	^{13}C	disordered
T $\pm$ 2 (°C)	1630 cm^{-1}	1616 cm^{-1}	1667 cm^{-1}	1630 cm^{-1}	1610 cm^{-1}	1667 cm^{-1}	1639 cm^{-1}	1618 cm^{-1}	1665 cm^{-1}
25	3.0 $\pm$ 2.9	5.5 $\pm$ 0.4	5.8 $\pm$ 0.5	3.7 $\pm$ 1.5	4.0 $\pm$ 0.6	5.4 $\pm$ 0.5	1.4 $\pm$ 0.2	3.6 $\pm$ 0.1	5.1 $\pm$ 0.5
30	2.3 $\pm$ 0.4	3.7 $\pm$ 0.2	3.4 $\pm$ 0.3	2.5 $\pm$ 0.2	2.8 $\pm$ 0.3	4.0 $\pm$ 0.4	1.4 $\pm$ 0.1	2.8 $\pm$ 0.1	4.9 $\pm$ 0.3
35	1.9 $\pm$ 0.2	3.5 $\pm$ 0.2	2.7 $\pm$ 0.1	2.0 $\pm$ 0.1	2.6 $\pm$ 0.2	3.0 $\pm$ 0.1	1.5 $\pm$ 0.4	2.5 $\pm$ 0.1	3.0 $\pm$ 0.2
40	1.6 $\pm$ 0.2	2.4 $\pm$ 0.1	1.9 $\pm$ 0.1	1.4 $\pm$ 0.1	2.0 $\pm$ 0.1	3.0 $\pm$ 0.2	1.4 $\pm$ 0.3	1.7 $\pm$ 0.1	2.4 $\pm$ 0.1
45	1.4 $\pm$ 0.2	1.8 $\pm$ 0.1	1.8 $\pm$ 0.1	1.6 $\pm$ 0.2	1.6 $\pm$ 0.1	2.0 $\pm$ 0.1	1.1 $\pm$ 0.3	1.4 $\pm$ 0.1	2.1 $\pm$ 0.1
50	1.0 $\pm$ 0.1	1.4 $\pm$ 0.1	1.1 $\pm$ 0.1	1.0 $\pm$ 0.1	1.2 $\pm$ 0.1	1.5 $\pm$ 0.1	1.0 $\pm$ 0.3	1.2 $\pm$ 0.1	1.2 $\pm$ 0.1

temperatures. Relaxation times derived at similar temperatures are additionally compared in Table 2.

At low temperatures the relaxation rates for different spectral bands are most distinct. Differentiation between strand-centered and disordered structure originating bands in the ^{12}C═O-based amide I′ modes, as noted above for the unlabeled Trpzip2C (Figure 4), is maintained in the thermal variation of the relaxation rates for component bands of the labeled compounds (Figure 5). At low temperatures (<40 °C), the ^{12}C═O β-hairpin band (blue) decays faster than the disordered band (red) appears in all three hairpins whereas little discrimination between relaxation times can be observed at high temperatures. This low-temperature region provides the distinct behaviors of amide I' modes for which we seek structural resolution with the site-specific isotopic label originating bands.

For **A3A10**, the variant with label positions closest together forming a 10-member H-bonded ring, the relaxation times of the ^{13}C═O band at 1610 cm^{-1} have a thermal variation that follows those of the ^{12}C═O band at ~1630 cm^{-1}, associated with the β-strand structure (Figure 5b). However, for the **A1A10** and **A3K8** variants, the ^{13}C═O band relaxation is different from the β-strand ^{12}C═O band. Both can form a large 14-member H-bonded ring, with the ^{13}C-labels closer to the termini in **A1A10** and closer to the turn in **A3K8**. In **A1A10**, the relaxation kinetics of the ^{13}C═O band at 1616 cm^{-1} follows the behavior of the ~1667 cm^{-1} band, which is characteristic of the unstructured component of the peptide. In **A3K8**, the relaxation kinetics of the ^{13}C═O band at 1618 cm^{-1} are faster than that of the ^{12}C═O band at 1665 cm^{-1} but slower than the β-strand band at 1639 cm^{-1}. Interestingly, the relaxation kinetics of the ^{12}C═O β-strand component band in **A3K8** seem to be faster at low temperature than the comparable bands in either **A1A10** or **A3A10**.

Comparison of the relaxation times of the ^{12}C═O β-strand, ^{13}C═O labeled, and the disordered band components measured at similar temperatures ($\pm$2 °C) for the different variants (Table 2) shows the decay dynamics of the ^{12}C═O β-strand component to be similar for **A1A10** and **A3A10,** considering the data error and temperature variations, but faster in **A3K8** at low temperatures. The relaxation times of the ^{13}C═O components tend to be similar for **A3K8** and **A3A10** but significantly slower for **A1A10**. The relaxation times for the rise of disordered structure behave similarly for all three variants when the larger error at low temperature is considered. It should be noted that the probed wavelengths for the β-strand and disordered bands of **A3K8** differ somewhat from the **A1A10** and **A3A10** since they have been selected based on the maximum absorption changes in the equilibrium measurements (Figure 3).

Activation energies have been determined by fitting the temperature-dependent relaxation data according to the Arrhenius equation and are summarized in Table 3. Comparing the decay of the ^{12}C═O β-strand bands, **A3K8** has the smallest activation energy, consistent with the relaxation times being fastest for this variant, and the **A3A10** variant and the unlabeled Trpzip2C have similar values. For the decay of the ^{13}C═O bands, the variant with the fastest relaxation times, **A3A10**, also shows the smallest activation energy. The activation energies are generally higher for the rise of the disordered bands than for the decay of the hairpin.

Table 3. Arrhenius Activation Energies, E_a,[a] for T-Jump Relaxation Kinetics for Trpzip2C and Labeled Variants

	^{12}C-strand		^{13}C		disordered	
	ν/cm^{-1}	E_a/kJ mol^{-1}	ν/cm^{-1}	E_a/kJ mol^{-1}	ν/cm^{-1}	E_a/kJ mol^{-1}
unlabeled	1625	27.8 $\pm$ 2.3			1661	33.2 $\pm$ 1.4
A1A10	1630	33.6 $\pm$ 1.9	1616	37.9 $\pm$ 1.4	1667	46.2 $\pm$1.3
A3A10	1630	28.9 $\pm$ 3.1	1610	29.6 $\pm$ 2.2	1667	41.4 $\pm$ 1.3
A3K8	1639	18.7 $\pm$ 4.1	1618	37.6 $\pm$ 0.9	1665	41.6 $\pm$ 2.5

[a] Determined with $\ln(k) = -E_a/(RT) + \ln(A)$.

Discussion

Although this paper presents the first application of site-specifically resolved T-jump IR to the study of hairpin folding and unfolding through the use of resolved cross-strand coupling of isotopically labeled residues, some T-jump measurements in combination with IR detection and isotopic labeling have been used to study α-helical peptides, and others have looked at unlabeled hairpin models.[4,8,27−29,35] Stability variations at different positions can be observed from the differences in folding dynamics for individual ^{13}C-shifted amide I′ bands. For the tryptophan hairpin peptides we have studied, isotopically shifted amide I′ bands have frequency and intensity characteristics that are highly sensitive to the labeling position, even more than for α-helical peptides.[6,12,14,15,36,37] The folding mechanisms of β-hairpin peptides containing tryptophans have been studied by T-jump measurements with infrared[4,28] or fluorescence[38,39] probes, detecting the backbone C═O groups or the tryptophan side chains, respectively. Structural studies on Trpzip2 have been initiated by Cochran et al.[22] with CD measurements in thermal equilibrium, ultracentrifugation, and NMR spectroscopy. A variety of further spectroscopic studies as IR,[23] femtosecond 2D-IR and dispersed vibrational echo spectroscopy,[24,25] T-jump

(35) Ramajo, A. R.; Petty, S. A.; Starzyk, A.; Decatur, S. M.; Volk, M. *J. Am. Chem. Soc.* **2005**, *127*, 13784−13785.
(36) Tadesse, L.; Nazarbaghi, R.; Walters, L. *J. Am. Chem. Soc.* **1991**, *113*, 7036−7037.
(37) Halverson, K. J.; Sucholeiki, I.; Ashburn, T. T.; Lansbury, P. T. *J. Am. Chem. Soc.* **1991**, *113*, 6701−6703.
(38) Muñoz, V.; Thompson, P. A.; Hofrichter, J.; Eaton, W. A. *Nature* **1997**, *390*, 196−199.
(39) Muñoz, V.; Ghirlando, R.; Blanco, F. J.; Jas, G. S.; Hofrichter, J.; Eaton, W. A. *Biochemistry* **2006**, *45*, 7023−7035.

IR absorption,[29] and T-jump Trp-fluorescence[26,29] as well as simulations[27,29,40−42] have been employed to analyze the thermal stability and folding mechanism.

Using T-jump IR absorption and T-jump Trp-fluorescence spectroscopy, Snow et al.[29] have determined the folding times of Trpzip2 to be 1.8 μs (fluorescence) and 2.47 μs (IR) and the unfolding times to be 18 μs (fluorescence) and 24.7 μs (IR) at 23 °C. Using a two-state model, the observed relaxation times would then be 1.6 μs (fluorescence) and 2.2 μs (IR). The molecular dynamics simulations accompanying that study determined folding rates for Trpzip2 that were in good agreement with their experimental data. It was concluded from the analysis of individual trajectories that the timing of events such as the formation of hydrogen bonds or tryptophan contacts was heterogeneous.

Yang et al.[27] used CD, IR, and fluorescence spectroscopy in combination with replica exchange molecular dynamics to study the folding energy landscape of Trpzip2 under varying temperature and denaturant (GdHCl) conditions. Unfolding transitions of Trpzip2 were observed and computed to be clustered in three general temperature regions. Multiple denatured ensembles, each with different properties, were observed as the temperature is lowered and the native state is populated. This behavior was explained by there being a rough energy landscape for the unfolded peptide caused by multiple tryptophan interactions and alternative backbone conformations. Further T-jump Trp-fluorescence studies of Yang and Gruebele[26] showed wavelength-dependent fluorescence kinetics due to different local minima of Trpzip2 microstructures on the free energy landscape. It was observed that Trpzip2 relaxation occurs at least in two kinetic phases in 0−2 M GdHCl, independent of the peptide concentration. The faster relaxation time occurs within the first 100 ns corresponding to more tryptophan mobility whereas the slower and wavelength-dependent μs phase was attributed to the break-up of the Trp−Trp minicore. In 2 M GuHCl and at 57 °C, relaxation times have been determined to be 2.1 μs probed at the red end of the spectrum, corresponding to the more solvent-exposed tryptophans, and to be 2.7 μs probed at the blue end of the spectrum. Those wavelength-dependent fluorescence relaxation rates have also been shown to be temperature-dependent. The dynamics speed up as the temperature is raised, which was interpreted as due to more extended structures being populated at higher temperatures, whereas more compact structures are trapped at low temperatures.[26,27]

We studied a derivative of the Trpzip2 hairpin peptide mutated at three residues, termed Trpzip2C, with labeling as ^{13}C═O on pairs of peptide groups on opposite strands. The **A3A10** variant, having labels bracketed by Trp's (which are at positions 2, 4, 9, and 11), has a well-resolved ^{13}C═O side band at 1608 cm^{-1}. Its ^{12}C═O band shifts to higher frequency (1637 cm^{-1}) compared with the unlabeled peptide because of disruption of the extended exciton coupling in the strands by the isotopic substitution. The **A3K8** variant also has a distinct ^{13}C═O band, but in this case it is more intense and higher in frequency than for the **A3A10**. This frequency difference has been shown to be due to the opposite sign of the coupling constant for the cross-strand labels which form a small (10-member) H-bonded ring, such as for **A3A10**, and those which form a larger (14-member) ring, such as **A3K8**.[5,19−21] The coupled modes that are out of phase across the strands lead to the larger dipole moment and larger IR intensity, so changing the coupling sign reverses the component of the exciton split pair that becomes more intense.[20,21] By contrast, the **A1A10** variant has two less well resolved ^{13}C bands (1625 and 1614 cm^{-1}) which reflect the partial unfolding of the terminal residues in the hairpin. Thermal unfolding can be monitored by the frequency shift of the ^{12}C band and by the intensity change of the ^{13}C bands. The temperature dependence of the ^{13}C═O band is in each case different from the ^{12}C═O dependence and reflective of its position in the hairpin, as will be discussed separately (Huang et al., to be submitted).[30] Such changes suggest that following the relaxation dynamics after a rapid shift of temperature with these different IR bands could yield insight into the (un)folding mechanism. The kinetics will be determined by the local structure stability resulting from bonding, hydrogen bonds and hydrophobic interactions.

The rate behavior at high-temperature (Figures 4 and 5) is the same for the IR components that are indicative of a loss of β-strand and of a rise of the disordered structure, which we interpret as due to the unfolding rates being kinetically controlled by the release of the hydrophobic collapse. We obtain a relaxation time for the decay of the β-strand-related band of Tripzip2C of 1.9 ± 0.1 μs at 25 °C and acidic pH that is in good agreement with the 2.2 μs relaxation deduced from the T-jump IR measurements for Trpzip2 at 23 °C and neutral pH.[29] In contrast, the behavior at low temperatures where the two relaxations diverge, with the loss of sheet being faster (lower relaxation time) than the rise of disorder, further confirm that unfolding and folding do not correspond to a two state mechanism, as previously proposed based on the difference of Trpzip2 dynamics as studied with IR and fluorescence T-jump techniques.[26,29] One interpretation of this difference with temperature is that the favored folding mechanism varies with changes in the free energy landscape as temperature increases, such that a partially unfolded intermediate is populated at lower temperatures, but contributions from intermediates become negligible at higher temperatures.

Stability variations at different positions can be observed from differences in folding dynamics for individual ^{13}C amide I′ bands. Differences in site-specific dynamics can be seen between the **A1A10**, **A3A10**, and **A3K8** (Figure 5). The decays of the β-strand ^{12}C bands represent the dynamics of disturbing the intact β-hairpin structure. In **A3A10**, where the ^{13}C═O groups form a small H-bonded ring in the middle of the hairpin, the ^{13}C-amide I′ band has the same temperature-dependent dynamics as the ^{12}C-amide I′ band component characteristic of β-strand, reflecting the stability of the center of the antiparallel strands due to the hydrophobic interactions. In contrast, the **A1A10** and **A3K8** variants have different ^{13}C═O relaxation dynamics. The **A1A10** ^{13}C-amide I′ band decay differs from the β-strand ^{12}C═O band component and coincides with the (slower) relaxation dynamics of the disordered structure, whereas the **A3K8** ^{13}C-amide I′ band decay lies between the relaxation dynamics of the ^{12}C-amide I′ band and disordered structure. In the former case, the **A1A10** residues are close to the terminal

(40) Pitera, J. W.; Haque, I.; Swope, W. C. *J. Chem. Phys.* **2006**, *124*, 141102−1-141102−4.
(41) Zagrovic, B.; Snow, C. D.; Khaliq, S.; Shirts, M. R.; Pande, V. S. *J. Mol. Biol.* **2002**, *323*, 153−164.
(42) Ulmschneider, J. P.; Jorgensen, W. L. *J. Am. Chem. Soc.* **2004**, *126*, 1849−1857.

groups and consequently, when labeled, are structurally more disordered and less cross-strand coupled than for the other two doubly labeled variants. Uncoupling of the labeled positions caused by fraying of the strands is reflected in the **A1A10** equilibrium amide I′ band shape pattern whose $^{13}C{=}O$ bands lie essentially at wavenumbers similar to those observed for singly labeled variants.[30] This behavior is consistent with loss of cross-strand coupling and a more unstructured conformation. Since the termini dynamics represent a mode of decay for the hairpin structure, even if only from a partially folded state, the $^{13}C{=}O$ band in **A1A10** reflects the dynamics of the frayed ends upon unfolding. Thus on heating, the local structure of the labels changes little, and the residues involved reflect the disordered segments of the molecule. On the other hand, the labels in **A3K8** are closer to the turn and demonstrate a clear cross-strand coupling seen by the distinct and intense coupled $^{13}C{=}O$ band (Figure 3d). However, the turn residues stress the hairpin structure, resulting in a distortion of the H-bond between positions 5 and 8. Also in the NMR Trpzip2 structure[22] the turn residues are not characterized by a well-formed cross-strand H-bond (from E5 C═O to K8 N−H). This distortion may influence the local unfolding kinetics. Thus, dynamics of the **A3K8** $^{13}C{=}O$ labeled band could reasonably reflect an intermediate kinetic behavior between the strand and disordered components.

The (faster) decay of the β-strand $^{12}C{=}O$ band component represents the break of the hydrophobic cross-strand interactions and loss of the β-hairpin structure as is monitored locally by the **A3A10** labels which are enclosed by the four tryptophans. Even though the Trp−Trp interactions cannot be probed by IR directly, an increased mobility of the tryptophan core part, as observed by fluorescence experiments,[26,27,29] will also lead to a loosening of the backbone structure in the hairpin core. Thus, the $^{13}C{=}O$ band component of **A3A10** reflects the stability loss of the center with the same dynamics as the $^{12}C{=}O$ band component. The hairpin termini, more selectively monitored by the **A1A10** labels, seem to be less sensitive to unfolding of the core, which becomes obvious when the partially unfolded state is populated. Since the termini dynamics represent a mode of decay for the hairpin structure, even if only from a partially folded state, the band arising from the **A1A10** labels reflects the dynamics of the frayed ends upon unfolding. **A3K8**, probing the hairpin part adjacent to the turn, shows kinetics of the ^{13}C-amide I′ mode to be slower that the $^{12}C{=}O$ amide I′ strand component of **A3K8**. In this variant, the ^{12}C-strand component decays faster than in the other two labeled variants.

Taken together, at low temperatures, **A3A10** reveals local $^{13}C{=}O$ amide I′ components with the same kinetics as the $^{12}C{=}O$ β-strand, whereas **A1A10** and **A3K8** both have $^{13}C{=}O$ relaxation kinetics that differ from those values. The $^{13}C{=}O$ kinetics are decelerated in the case of **A1A10** to match the kinetics of the disordered component. The labels of **A1A10** and **A3K8** sense more of the dynamics of the unfolded state whereas the **A3A10** labels sense the disruption of the fully intact segment of the β-hairpin backbone structure in the core. It is quite likely that in the particular low-temperature region that we probed in this study, the hydrophobic contacts of the tryptophans in the hairpin core are partially maintained while the backbone contacts start to denature. This is somewhat supported by the residual CD signal, characteristic of Trp−Trp interaction, that can be seen at high temperature. Together, the thermodynamic and kinetic data suggest an enduring role for the hydrophobic interaction between Trp residues. The faster (more β-strand like) $^{13}C{=}O$ kinetics of the **A3A10** variant suggests that the central part of the strand, where the Trps are in the sequence, is the stable component. This suggests that unfolding progresses from the termini and turn toward the center. This is the type of unfolding behavior we have seen in model MD calculations for similar hairpin structures[19] (Kim and Keiderling, unpublished results). By microscopic reversibility, this would support that folding is initiated by a hydrophobic collapse. Such reversibility would only be tenable where the model is experimentally valid at high temperatures, since at low temperatures the divergence of relaxation kinetics suggests the formation of an intermediate and non-two-state behavior. Although the site-specificity of the relaxation times could only be obtained at low temperatures from a partially folded state, the data is still supportive for this hypothesis.

Conclusion

Our results show the potential of T-jump kinetics in combination with isotopic labeling to determine site-specific conformational dynamics in peptides. Differences in relaxation times between the ^{12}C- and ^{13}C-amide I′ bands can reflect localized structure dynamics, but each can also affect the other in terms of exciton coupling. We interpret the spectral response of the probed label positions as indication for a hydrophobic collapse-mediated hairpin folding mechanism. Since the site-specific kinetics only become differentiated at low temperatures, where substantial Trp−Trp interaction remains, they also could reflect a re-equilibration of the backbone from a loosened, but still structured, hydrophobic core. Nevertheless, the isotope-edited amide I′ relaxation kinetics show differences in local structural stability of the backbone that should become even more dominant at high temperatures.

Acknowledgment. This work was supported by the Ministry of Science and Culture of Hesse (HMWK) and by an NSF grant (CHE03-16014, 07-18543 to T.A.K.), and the collaboration was initiated through a Fellowship to T.A.K. from the John Simon Guggenheim Memorial Foundation. We thank Dr. Dan McElheny, UIC, for help obtaining and assigning the NMR data.

JA074215L